

Targeted protein unfolding uncovers a Golgi-specific transcriptional stress response

Yevgeniy V. Serebrenik^{a,†}, Doris Hellerschmied^{a,†}, Momar Toure^b, Francesc López-Giráldez^c, Dennis Brookner^a, and Craig M. Crews^{a,b,d,*}

^aDepartment of Molecular, Cellular and Developmental Biology, ^bDepartment of Chemistry, and ^dDepartment of Pharmacology, Yale University, New Haven, CT 06511; ^cYale Center for Genome Analysis, Yale University School of Medicine, New Haven, CT 06520

ABSTRACT In eukaryotic cells, organelle-specific stress-response mechanisms are vital for maintaining cellular homeostasis. The Golgi apparatus, an essential organelle of the secretory system, is the major site of protein modification and sorting within a cell and functions as a platform for spatially regulated signaling. Golgi homeostasis mechanisms that regulate organelle structure and ensure precise processing and localization of protein substrates remain poorly understood. Using a chemical biology strategy to induce protein unfolding, we uncover a Golgi-specific transcriptional response. An RNA-sequencing profile of this stress response compared with the current state-of-the-art Golgi stressors, nigericin and xyloside, demonstrates the enhanced precision of Golgi targeting achieved with our system. The data set further reveals previously uncharacterized genes that we find to be essential for Golgi structural integrity. These findings highlight the Golgi's ability to sense misfolded proteins and establish new aspects of Golgi autoregulation.

Monitoring Editor
Anne Spang
University of Basel

Received: Nov 30, 2017
Revised: Mar 26, 2018
Accepted: Mar 30, 2018

INTRODUCTION

The Golgi apparatus is a complex organelle that orchestrates many important functions in eukaryotic cells. As the central member of the secretory pathway, the Golgi is a major site of protein

This article was published online ahead of print in MBoC in Press (<http://www.molbiolcell.org/cgi/doi/10.1091/mbc.E17-11-0693>) on April 5, 2018.

[†]These authors contributed equally to this work.

Author contributions: Y.V.S., D.H., and C.M.C. designed the study and interpreted the data; Y.V.S. and D.H. performed tissue culture and cell line generation, immunoblotting, and immunofluorescence; Y.V.S., D.H., and D.B. generated DNA constructs; F.L.-G. processed RNA-sequencing data, which were analyzed by Y.V.S., D.H., and F.L.G.; Y.V.S. performed qPCR, flow cytometry, and cell toxicity experiments; D.H. performed limited proteolysis, and M.T. performed the chemistry; Y.V.S., D.H., and C.M.C. wrote and edited the article.

Competing financial interests: C.M.C. is a consultant to and a shareholder in Arvina, LLC, which supports research in the Crews lab.

*Address correspondence to: Craig M. Crews (craig.crews@yale.edu).

Abbreviations used: ANOVA, analysis of variance; DAPI, 4',6-diamidino-2-phenylindole; EM, electron microscopy; ER, endoplasmic reticulum; ESI, electrospray ionization; FBS, fetal bovine serum; HRP, horseradish peroxidase; HT2, HaloTag2; PBS, phosphate-buffered saline; qPCR, quantitative PCR; RFP, red fluorescent protein; shRNA, short hairpin RNA; ssHRP, secretory signal HRP; THF, tetrahydrofuran.

© 2018 Serebrenik, Hellerschmied, et al. This article is distributed by The American Society for Cell Biology under license from the author(s). Two months after publication it is available to the public under an Attribution–Noncommercial–Share Alike 3.0 Unported Creative Commons License (<http://creativecommons.org/licenses/by-nc-sa/3.0>).

"ASCB®," "The American Society for Cell Biology®," and "Molecular Biology of the Cell®" are registered trademarks of The American Society for Cell Biology.

modification and sorting (De Matteis and Luini, 2008; Morre and Mollenhauer, 2009; Lippincott-Schwartz and Phair, 2010; Brandizzi and Barlowe, 2013; Progida and Bakke, 2016). Throughout the Golgi, proteins imported from the endoplasmic reticulum (ER) can acquire many posttranslational modifications, including the addition or removal of carbohydrates (Morre and Mollenhauer, 2009; Stanley, 2011; Moremen et al., 2012). These modifications occur without the use of templates and rely on the precise control of Golgi compartmentalization, reaction rates, and substrate/product concentrations (Varki, 1998; Stanley, 2011). Proteins destined to leave the Golgi are packaged into specific carriers for targeted trafficking to various cell compartments (De Matteis and Luini, 2008; Progida and Bakke, 2016). Golgi trafficking and processing events are tightly integrated with signaling pathways, such as those driven by Src and PKA, which can directly influence secretion and Golgi structural integrity (Muñiz et al., 1997; Martin et al., 2000; Cabrera et al., 2003; Bejarano et al., 2006; Pulvirenti et al., 2008; Mavillard et al., 2010; Giannotta et al., 2012). Moreover, the Golgi can serve as an assembly platform for major signaling complexes (Farhan and Rabouille, 2011; Mayinger, 2011; Makowski et al., 2017).

The structure and function of the Golgi change during different stages of the cell cycle and also during conditions of stress. Regulated structural disassembly occurs during cell division, after which

the Golgi is reassembled in daughter cells (Shorter and Warren, 2002; Sütterlin *et al.*, 2002; Corda *et al.*, 2012). Additionally, the demands of increased protein secretion can influence Golgi size and capacity (Bierring, 1962; Rambourg *et al.*, 1987). Stress related to disease can also alter Golgi structure (Bexiga and Simpson, 2013). In particular, a dispersed Golgi phenotype has been observed in several cancer cell lines and may play a central role in metastasis (Kellokumpu *et al.*, 2002; Baschieri *et al.*, 2014, 2015; Petrosyan *et al.*, 2014). Additionally, in Alzheimer's disease, the Golgi is known to undergo fragmentation, and it is thought that fortifying Golgi stability could be a potential therapeutic strategy (Stieber *et al.*, 1996; Jiang *et al.*, 2014; Joshi *et al.*, 2014). Thus, to ensure proper function of Golgi processes not only basally but also during stress, the requirement for dedicated stress-response and homeostatic mechanisms is readily apparent.

Knowledge of Golgi homeostatic mechanisms is sparse due to limitations of current tools used to perturb and study the Golgi. Various pharmacological agents interfering with Golgi functions, such as ionophores (e.g., monensin and nigericin) that increase the pH of acidic endomembrane compartments, glycosylation inhibitors (e.g., xyloside and GalNAc-bn), and brefeldin A, which interferes with Golgi-related transport processes, have been used to induce Golgi stress (Oku *et al.*, 2011; Miyata *et al.*, 2013; Reiling *et al.*, 2013; Taniguchi *et al.*, 2015; Baumann *et al.*, 2017). However, these stressors are not Golgi specific and possess a multitude of confounding effects, that is, ionophores affect the pH of several organelles, and glycosylation inhibitors affect many downstream processes involving glycosylated proteins (Okayama *et al.*, 1973; Hamati *et al.*, 1989; Mollenhauer *et al.*, 1990; Freeze *et al.*, 1993; Dinter and Berger, 1998). Thus, it is difficult to identify direct consequences of Golgi stress and mechanisms that directly influence Golgi homeostasis.

To overcome these limitations, we have developed a novel chemical biology-based cell system that allows us to precisely stress the Golgi with minimal nonspecific effects. Our approach is based on induced protein unfolding via small-molecule hydrophobic tagging of a HaloTag fusion protein, a strategy that has been used to study protein quality-control and stress-response mechanisms in the cytosol and ER (Neklesa *et al.*, 2011, 2013; Encell *et al.*, 2012; Tae *et al.*, 2012; Raina *et al.*, 2014). Here, we explore the transcriptional changes induced by nigericin, xyloside, and our protein unfolding-based system, thereby demonstrating that the selective and targeted unfolding of a Golgi-localized protein affects the Golgi with greater precision when compared with tool compounds currently used to study Golgi stress. We further characterize this Golgi stress transcriptional response to reveal novel genes that are vital for Golgi structural integrity. Furthermore, since our system is based on protein unfolding, we also report the novel finding that the Golgi apparatus has a dedicated response to protein unfolding.

RESULTS AND DISCUSSION

Development of a protein-unfolding system in the Golgi

Given the complex processes that occur within the Golgi apparatus and the importance of a functioning proteome for their fidelity, we hypothesized that protein misfolding would be capable of disturbing Golgi homeostasis. To this end, we used the hydrophobic tagging technology based on the HaloTag domain (Los *et al.*, 2008; Encell *et al.*, 2012). The HaloTag domain is derived from a bacterial dehalogenase and can covalently conjugate to chloroalkanes such as hydrophobic tags, which can induce HaloTag destabilization (Neklesa *et al.*, 2011; Tae *et al.*, 2012). We previously showed that destabilization of HaloTag2 (HT2) fusion proteins in the cytosol or the ER by hydrophobic tagging leads to degradation of the HT2

fusion protein and to the induction of cellular stress-response pathways (Neklesa *et al.*, 2011, 2013; Raina *et al.*, 2014). Prior studies have also demonstrated that the hydrophobic tag, HyT36, directly reduces protein stability of HaloTag7 *in vitro* (Tae *et al.*, 2012). To gain insight into the destabilization of HT2 proteins by hydrophobic tagging, we monitored the effect of HyT36 on a luciferase-HT2 fusion construct *in vitro*. We synthesized a des-chloro derivative of HyT36, HyT36(-Cl) that is unable to bind HaloTag and serves as a negative control (Figure 1A). Activity assays upon treatment with HyT36, HyT36(-Cl) or vehicle control clearly demonstrate that conjugation of the hydrophobic tag to luciferase-HT2 leads to protein misfolding (Supplemental Figure S1A).

To explore homeostasis mechanisms in the Golgi apparatus, we designed enhanced green fluorescent protein (EGFP)-HT2 fusion protein localized to the Golgi apparatus (GA-HT2) via the transmembrane domain of the Golgi-resident protein B4GALT1 (Figure 1A). Induced expression of the construct in either HEK293 or HeLa Flp-In T-REx cell lines upon doxycycline treatment led to proper localization of the fusion protein as visualized by colocalization with the Golgi marker giantin (Figure 1B). Protein destabilization was induced using the HyT36 hydrophobic tag (Tae *et al.*, 2012). Using a limited proteolysis assay, we confirmed that GA-HT2 is susceptible to HyT36-mediated destabilization. Specifically, HyT36 treatment increased GA-HT2 sensitivity to trypsin digestion in cell lysates (Figure 1C). Unlike the protein levels of cytosolic and ER-localized HT2 (Neklesa *et al.*, 2011; Tae *et al.*, 2012; Raina *et al.*, 2014), protein levels of GA-HT2 were not reduced following HyT36 treatment, as measured by Western blotting (Figure 1D) and flow cytometry, even in the presence of cycloheximide and at extended incubation times (Supplemental Figure S1B). Conversely, HyT36 caused a slight increase (~20–30%) in GA-HT2 protein levels compared with control, which is attributed to clonal variability. As expected, GA-HT2 mRNA levels also remained constant over time during HyT36 treatment (Supplemental Figure S1C). Hydrophobic tagging of HT2 fusion proteins in HeLa cells followed the same pattern of localization-dependent sensitivity to degradation as in HEK293 cells (Neklesa *et al.*, 2011; Tae *et al.*, 2012; Raina *et al.*, 2014); while HyT36 did not affect the levels of Golgi-localized HT2, unfolded cytosolic and ER-localized HT2 fusion proteins were degraded (Supplemental Figure S1D).

Having established an inducible Golgi-specific protein-unfolding system, we compared its cellular effects with those of other Golgi stressors. In contrast to most other strategies used to study Golgi stress (e.g., nigericin treatment), hydrophobic tagging of GA-HT2 at 10 μ M HyT36 is nontoxic and does not disrupt Golgi morphology. Toxicity was measured by cell counting after 24 h exposure of GA-HT2 HEK293 cells to various treatments (Supplemental Figure S1E). Nigericin caused an ~55% reduction in cell number relative to control. Conversely, HyT36 had no effect on cell numbers in the absence of GA-HT2 expression, and in the presence of GA-HT2, HyT36 caused a nonsignificant reduction relative to HyT36(-Cl). Furthermore, hydrophobic tagging of GA-HT2 did not lead to any detectable ultrastructural changes in Golgi morphology compared with control in HeLa cells, as measured by transmission electron microscopy (Supplemental Figure S1F). Taken together, these results show that the GA-HT2 hydrophobic tagging system is well suited for studying Golgi-specific stress without the confounding effects of severe organelle disruption or cell death.

Protein destabilization in the Golgi elicits a unique and specific transcriptional response

Typically, organelle-specific stress responses are characterized by changes in gene expression that increase the functional capacity

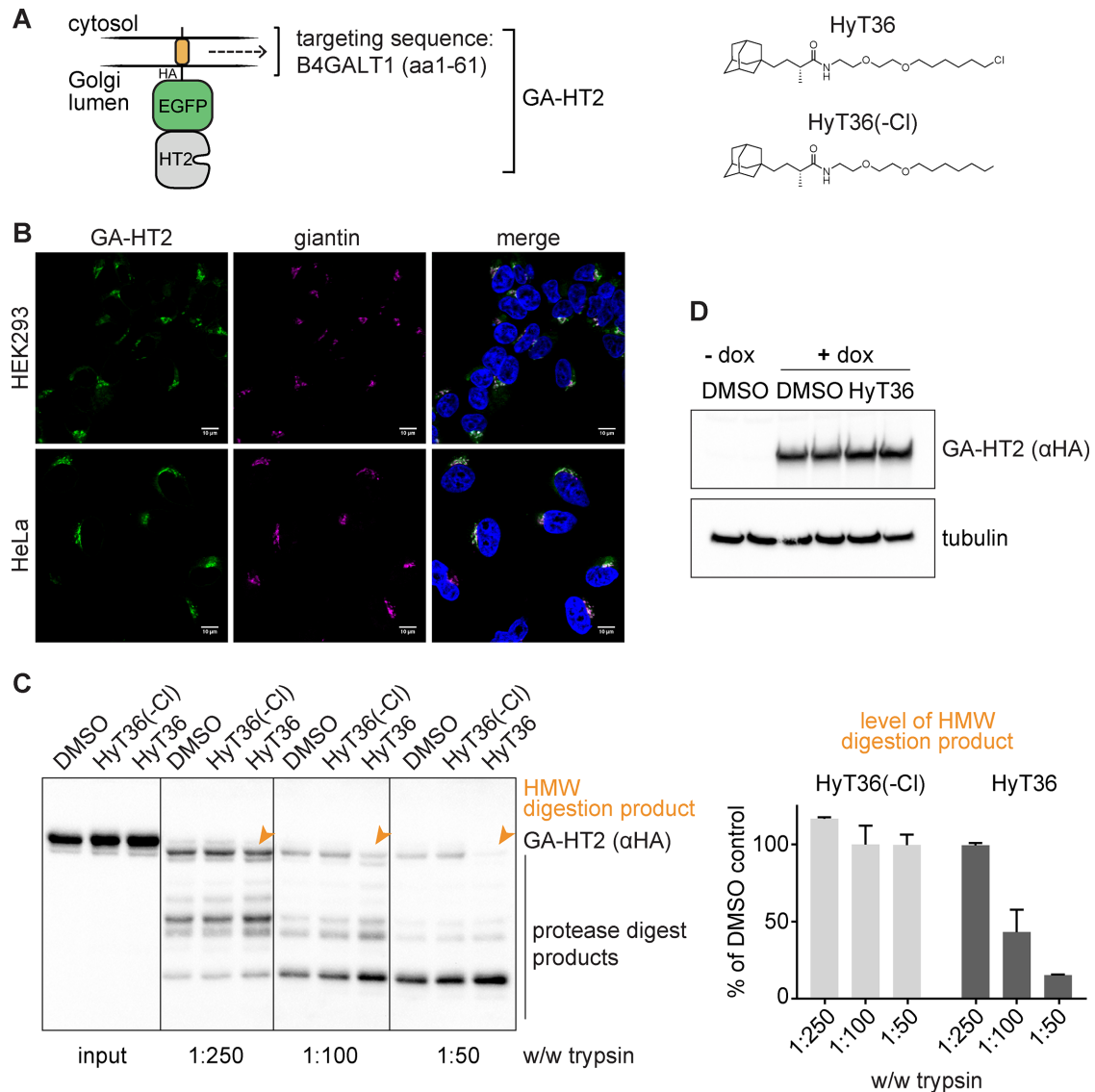


FIGURE 1: The hydrophobic tagging system for protein destabilization in the Golgi. (A) Schematic of the GA-HT2 construct and chemical structures of the hydrophobic tag, HyT36, and control molecule, HyT36(-Cl). (B) Representative confocal microscopy images of GA-HT2 (green) colocalization with giantin (magenta) in HEK293 and HeLa cells. Nuclei are visualized with 4',6-diamidino-2-phenylindole (DAPI; blue). Scale bar: 10 μm. (C) Left, representative Western blot of limited proteolysis of GA-HT2 HEK293 cells after treatment with HyT36, HyT36(-Cl), or DMSO. Right, quantitation of the high-molecular-weight (HMW) digestion product for HyT36 and HyT36(-Cl). Levels are normalized to DMSO control. Data represent mean ± SD ($n = 2$). (D) Western blot showing total GA-HT2 levels in HEK293 cells in duplicate after 24 h of doxycycline treatment followed by 8 h of HyT36 or DMSO treatment.

of the organelle. We hypothesized that a possible transcriptional response to protein misfolding in the Golgi would have genes in common with other stress responses induced by agents such as ionophores or glycosylation inhibitors (Oku *et al.*, 2011; Taniguchi *et al.*, 2015). Accordingly, we examined the ability of hydrophobic tagging in the Golgi to up-regulate genes known to be involved in Golgi structure and trafficking, such as the structural protein and tether GM130 and the SNARE STX3A, which have previously been shown to be responsive to Golgi stressors, including nigericin and xyloside (Oku *et al.*, 2011; Taniguchi *et al.*, 2015). As measured by quantitative PCR (qPCR), hydrophobic tagging induces changes in the expression of the same gene set previously reported to be induced by nigericin or xyloside treatment (Figure 2A). As expected, this response was dependent not only on expression of

GA-HT2, but also on conjugation of the hydrophobic tag to the HT2 domain, as demonstrated by comparison to HyT36(-Cl) (Supplemental Figure S2A). Hydrophobic tagging of GA-HT2 also induced up-regulation of Golgi stress genes in HeLa cells, demonstrating the generality of this response among cell lines (Supplemental Figure S2B). To assess the dynamic range of stress gene induction, we performed qPCR experiments at a lower doxycycline concentration, which induced ~45% lower GA-HT2 expression for the entire population of treated cells (Supplemental Figure S2C). These experiments reveal that the fold induction of stress genes scales with GA-HT2 expression levels (Supplemental Figure S2D). Moreover, when GA-HT2-expressing cells are treated with the HT2 stabilizer HALTS1 (Neklesa *et al.*, 2013), the expression of some stress genes is reduced compared with control conditions,

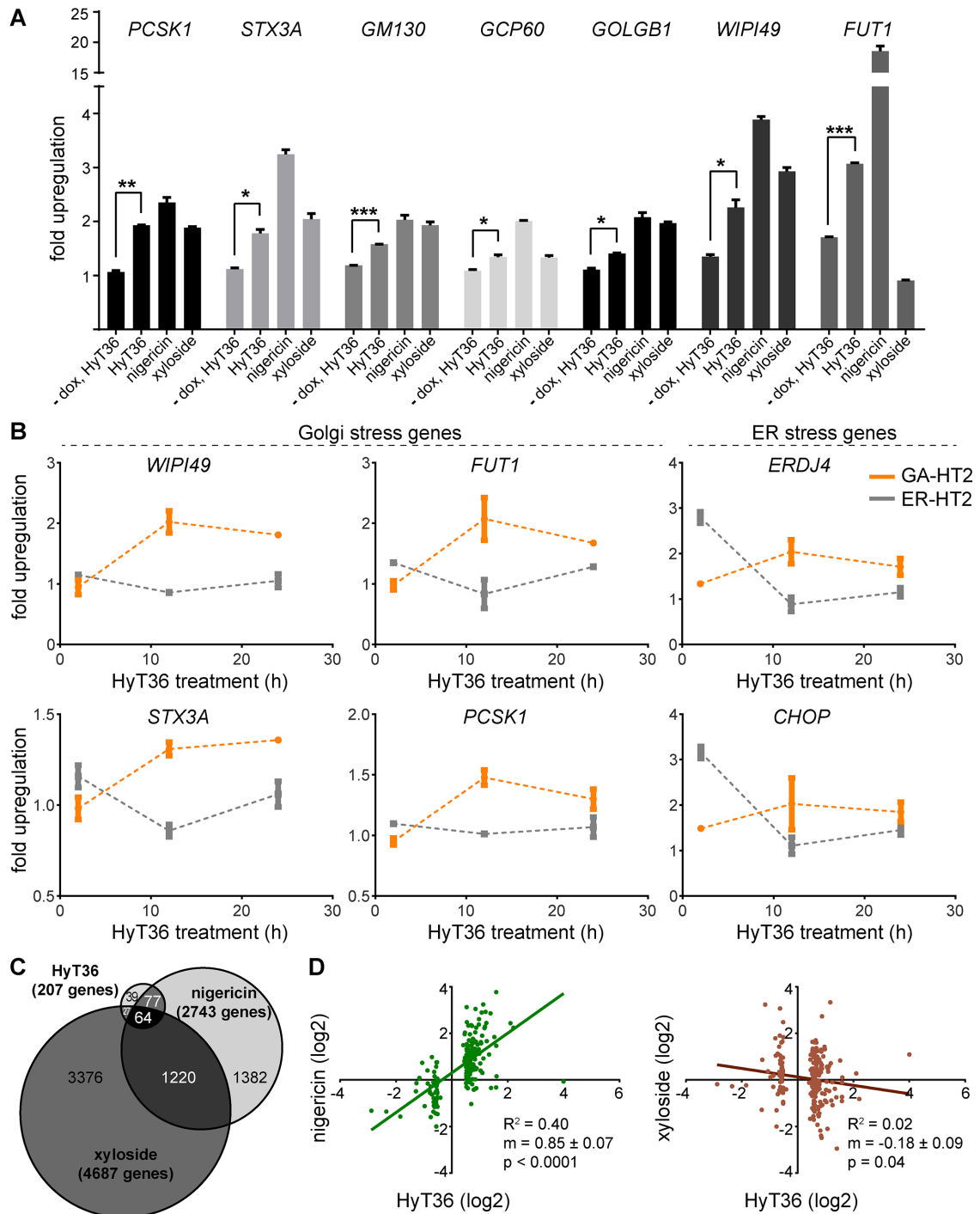


FIGURE 2: Destabilization of GA-HT2 induces a specific Golgi stress response. (A) qPCR of Golgi stress genes in HEK293 cells treated for 12 h with HyT36 in the absence or presence of doxycycline or with nigericin or xyloside in the absence of doxycycline. Fold up-regulation over DMSO control is shown. Data represent mean \pm SEM ($n = 2$). *, $p < 0.05$; **, $p < 0.01$; ***, $p < 0.001$ (t test). (B) qPCR time course of selected Golgi and ER stress genes after treatment with HyT36 for 2, 12, and 24 h in HEK293 cells. Fold up-regulation with HyT36 over HyT36(-Cl) is shown. Data represent mean \pm SEM ($n = 2$). (C) Venn diagram summarizing the overlap of genes significantly affected by a 12-h treatment with HyT36, nigericin, or xyloside. Significant genes were counted as those with an experimental log ratio of at least 0.5 and a maximum false-discovery rate of 0.06. (D) Correlation plots of significant genes identified by HyT36 treatment compared with their fold change induced by nigericin or xyloside.

effectively increasing the dynamic range of the Golgi stress transcriptional response and further highlighting the relationship between GA-HT2 stability and stress gene expression levels (Supplemental Figure S2D).

To explore the relationship between the transcriptional response to HT2 unfolding in the Golgi and the unfolded protein response in the ER, we generated an analogous dox-inducible ER-HT2 cell line using a signal sequence derived from calreticulin and a C-terminal

KDEL sequence, akin to the constitutive ER-HT2-expressing cell line used previously (Raina *et al.*, 2014). Having established the GA- and ER-HT2 cell lines, we compared the kinetics of up-regulation of several Golgi and ER stress genes by qPCR after HyT36 treatment. Remarkably, the analyzed Golgi stress genes (*WIPI49*, *FUT1*, *PCSK1*, and *STX3A*) were activated only in the GA-HT2 cell line, peaking at around 12 h. These results suggest that this transcriptional response to protein misfolding-related stress is a unique response of the Golgi apparatus (Figure 2B). Furthermore, the GA-HT2 cell line shows only minimal up-regulation of the ER stress genes *CHOP* and *ERDJ4* at their peak activation time of 2 h, as compared with the ER-HT2 line, thus emphasizing the specificity of the GA-HT2 system toward Golgi stress. Interestingly, we observed a slight up-regulation of ER stress genes in the GA-HT2 line at 12 h, suggesting possible cross-talk between the two stress responses. In summary, hydrophobic tagging of a Golgi-localized HT2 protein allowed us to uncover a unique and specific response to protein unfolding in the Golgi apparatus.

RNA sequencing was performed to enable a broader understanding of how the Golgi stressors nigericin, xyloside, and HyT36-induced HT2 unfolding influence transcription (Supplemental Table S1). HyT36 treatment significantly affected 207 genes with an experimental log ratio threshold of 0.5, while nigericin affected 2743 genes and xyloside affected 4687 genes under the same constraints (Figure 2C). HyT36 treatment affects the smallest subset of target genes, reinforcing that it is a more specific stressor than either nigericin or xyloside. We examined the similarity between HyT36 and the other stressors by comparing the fold change of the 207 genes affected by HyT36 to their fold change under nigericin or xyloside treatment. While there was no obvious relationship with xyloside, HyT36 exhibited a strong correlation with nigericin (Figure 2D). Notably, the slope of the correlation is close to 1, suggesting that HyT36 acts just as potently as nigericin in terms of inducing Golgi stress. This observation further suggests a mechanistic similarity between the types of Golgi stress induced by the two treatments. It is possible that at least one of the effects of nigericin on the Golgi is to induce protein destabilization, given its impact on the pH of the Golgi lumen and on protein transport bulk flow (Dinter and Berger, 1998). Conversely, there is no correlation between GA-HT2 destabilization and xyloside treatment, suggesting that xyloside may be inducing a different type of Golgi stress compared with that resulting from HyT36-induced protein destabilization and nigericin treatment.

The RNA-sequencing data sets provide insight into the effects of the small-molecule stressors on cells. To this end, a Gene Ontology term analysis underscored the specificity of the GA-HT2/HyT36 system to the Golgi apparatus. Categorizing the genes significantly affected by the three stressors revealed an enrichment of Golgi-associated genes in the HyT36 data set. In contrast, nigericin and xyloside both appeared to have broad cellular effects (Table 1). Together, these data show that HyT36-induced unfolding of GA-HT2 produces a transcriptional Golgi-specific stress signature that is similar to a part of the cellular effect of nigericin.

Identification of novel genes essential for Golgi structural integrity

Many of the genes that are induced in response to HyT36 treatment, such as *GOLGA5*, *GOLGB1*, *GCP60* (*ACBD3*), and *GM130* (*GOLGA2*), are highly Golgi specific and are involved in maintaining Golgi homeostasis during stress (Diao *et al.*, 2003; Satoh *et al.*, 2003; Barinaga-Rementeria Ramirez and Lowe, 2009). Therefore, we reasoned that the previously uncharacterized genes identified as being up-regulated by the GA-HT2/HyT36 system may also play a

role in maintaining Golgi structural integrity. Of particular interest were genes predicted to be part of the secretory system, which may be directly involved in structural maintenance, as well as potential transcriptional regulators of the stress response. We confirmed by qPCR that HyT36 and nigericin induce the up-regulation of the previously uncharacterized genes *FAM174B*, *LYSMD3*, *ZNF501*, and *ZNF643* in GA-HT2 HEK293 cells (Supplemental Figure S3A). To assess changes in protein levels, we performed Western blot analysis. Changes induced by HyT36 treatment are too small to be consistently detected; however, nigericin treatment increases overall levels of *LYSMD3* in HEK293 cells, and this trend is also observed in HeLa cells (Supplemental Figure S3B). Moreover, nigericin treatment shifts the *LYSMD3* band from a higher-molecular-weight form to a band that corresponds to the size of the unmodified protein, suggesting a defect in secretory pathway function. Notably, in HEK293 cells, expression of GA-HT2 by doxycycline treatment also increases the levels of *LYSMD3*.

We next examined the effect of lentiviral short hairpin RNA (shRNA) knockdown of *FAM174B*, *LYSMD3*, *ZNF501*, and *ZNF643* on Golgi morphology and function. Knockdown of the targeted genes was confirmed by qPCR (and a Western blot for *LYSMD3*) in HEK293 and HeLa cell lines following viral transduction, although *FAM174B* and *ZNF501* mRNA were undetectable in HeLa cells (Supplemental Figure S3C). Indeed, knockdown of these selected genes resulted in major changes in Golgi structure, both in HEK293 and HeLa cell lines (Figure 3A and Supplemental Figure S4A). Using giantin immunofluorescence to visualize the Golgi, we observed significantly more fragmentation in shRNA-expressing cells than in non-hairpin shRNA control cells. To quantify this morphological change, we determined the Golgi compactness index from projections of z-stack images as previously described (Figure 3B) (Bard *et al.*, 2003). Ultrastructural changes in Golgi morphology were further monitored by electron microscopy (EM) (Supplemental Figure S4, B and C). The high-resolution images show that the Golgi cisternae are enlarged and swollen in the knockdown cell lines. To evaluate whether the observed Golgi disruption affects protein transport along the secretory pathway, we monitored secretion of the model substrate HRP (ssHRP). These experiments revealed that knockdown of *LYSMD3* reduces secretion in HeLa cells (Figure 3C). Additionally, knockdown of *ZNF501* reduces secretion in HEK293 cells (Supplemental Figure S4D), a trend that is also observed in HeLa cells (Figure 3C).

The stable shRNA cell lines could be cultured for multiple passages, despite disruption of the organelle and reduced protein transport capacity. To test whether knockdown of the newly identified Golgi stress genes would sensitize cells to treatment with nigericin, we carried out cell viability assays (Figure 3D). The knockdown cell lines did not show reduced viability in the presence of nigericin compared with the non-hairpin control cell line, suggesting that deletion of these individual Golgi stress-response genes is not sufficient to sensitize cells to nigericin or that the cytotoxic effect of the ionophore is not related to Golgi stress.

In silico analysis of *LYSMD3* and *FAM174B* predicts that both proteins contain a transmembrane domain and that the latter additionally harbors an N-terminal signal sequence for cotranslational import into the ER (Figure 3E). We determined their subcellular localization by expression of red fluorescent protein (RFP) fusion constructs in HeLa cells (Figure 3E). RFP-*LYSMD3* was primarily found at the Golgi apparatus and occasionally at the plasma membrane, depending on its expression level. *FAM174B*-RFP localized to the Golgi, to the plasma membrane, and to punctate structures distributed throughout the cytoplasm, pointing to a possible role in vesicular transport. Moreover, we found the two zinc-finger proteins

Rank	HyT36			Nigericin			Xyloside		
	Term ID	Term	logP	Term ID	Term	logP	Term ID	Term	logP
1	GO:0005794	Golgi apparatus	-7.27	GO:0044424	Intracellular part	-94.92	GO:0005622	Intracellular	-122.98
2	GO:0012505	Endomembrane system	-6.92	GO:0005622	Intracellular	-91.58	GO:0044424	Intracellular part	-119.21
3	GO:0044420	Extracellular matrix part	-6.70	GO:0043229	Intracellular organelle	-65.17	GO:0043229	Intracellular organelle	-87.34
4	GO:0005719	Nuclear euchromatin	-6.69	GO:0043226	Organelle	-59.93	GO:0043226	Organelle	-83.98
5	GO:0005581	Collagen trimer	-6.35	GO:0043231	Intracel. membrane-bd. orgl.	-57.98	GO:0043227	Membrane-bd. orgl.	-78.50
6	GO:0005604	Basement membrane	-6.25	GO:0043227	Membrane-bd. orgl.	-53.23	GO:0043231	Intracel. membrane-bd. orgl.	-78.05
7	GO:0000791	Euchromatin	-6.19	GO:0005737	Cytoplasm	-43.40	GO:0005737	Cytoplasm	-67.65
8	GO:0030127	COPII vesicle coat	-5.72	GO:0044444	Cytoplasmic part	-39.09	GO:0044446	Intracellular organelle part	-40.63
9	GO:0043227	Membrane-bd. orgl.	-5.32	GO:0044446	Intracellular organelle part	-36.24	GO:0044444	Cytoplasmic part	-40.24
10	GO:0032587	Ruffle membrane	-5.31	GO:0044422	Organelle part	-34.27	GO:0044422	Organelle part	-38.25
11	GO:0005578	Proteinaceous ECM	-5.29	GO:0005829	Cytosol	-33.08	GO:0044464	Cell part	-38.00
12	GO:0044424	Intracellular part	-5.25	GO:0044464	Cell part	-28.90	GO:0005623	Cell	-37.80
13	GO:0005783	Endoplasmic reticulum	-5.10	GO:0005623	Cell	-28.78	GO:0005634	Nucleus	-34.62
14	GO:0005622	Intracellular	-4.66	GO:0031981	Nuclear lumen	-22.50	GO:0070013	Intracellular organelle lumen	-23.45
15	GO:0005595	Collagen type XII trimer	-4.62	GO:0005634	Nucleus	-22.14	GO:0044428	Muclear part	-22.75
16	GO:0005585	Collagen type II trimer	-4.62	GO:0070013	Intracellular organelle lumen	-22.01	GO:0043233	Organelle lumen	-21.68
17	GO:0043231	Intracel. membrane-bd. orgl.	-4.44	GO:0031974	Membrane-enclosed lumen	-21.35	GO:0005856	Cytoskeleton	-21.39
18	GO:0043226	Organelle	-4.32	GO:0043233	Organelle lumen	-20.85	GO:0031974	Membrane-enclosed lumen	-21.09
19	GO:0031012	Extracellular matrix	-4.16	GO:0044428	Nuclear part	-18.23	GO:0005912	Adherens junction	-19.99
20	GO:0048770	Pigment granule	-4.15	GO:0043228	Nonmembrane-bd. orgl.	-16.27	GO:0043228	Nonmembrane-bd. orgl.	-19.65
21	GO:0042470	Melanosome	-4.15	GO:0043232	Intracel. nonmbr-bd. orgl.	-16.27	GO:0043232	Intracel. nonmbr-bd. orgl.	-19.65
22	GO:0044431	Golgi apparatus part	-3.93	GO:0005654	Nucleoplasm	-15.29	GO:0012505	Endomembrane system	-18.94
23	GO:0005615	Extracellular space	-3.83	GO:0015630	Microtubule cytoskeleton	-14.40	GO:0031981	Nuclear lumen	-18.92
24	GO:0000139	Golgi membrane	-3.71	GO:0031090	Organelle membrane	-12.73	GO:0005829	Cytosol	-18.55
25	GO:0030662	Coated vesicle membrane	-3.65	GO:0005815	Microtubule organizing center	-12.21	GO:0070161	Anchoring junction	-16.68

TABLE 1: Gene Ontology cellular compartment analysis of significant genes from RNA sequencing (top 25).

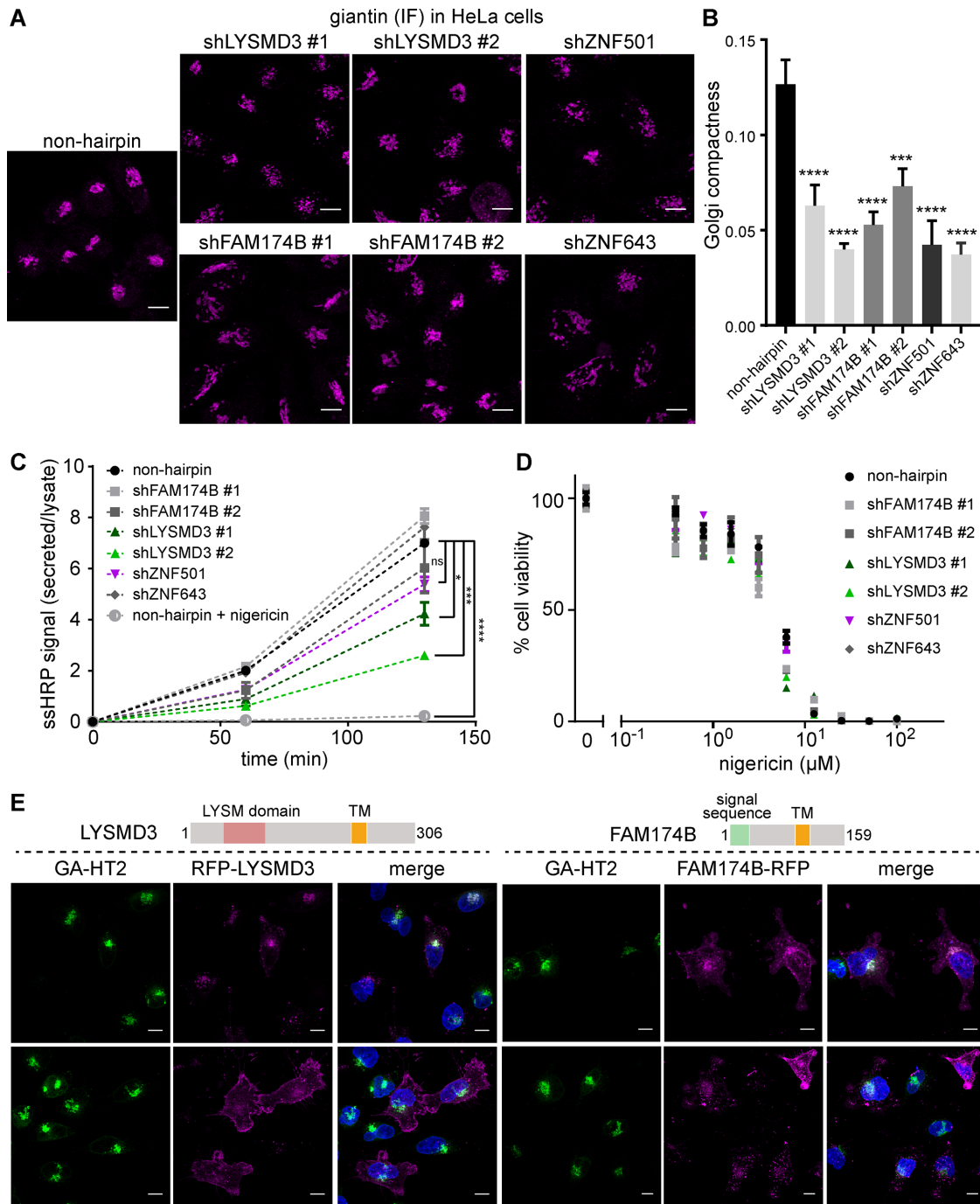


FIGURE 3: Novel Golgi stress genes are involved in Golgi integrity and secretion. (A) Representative giantin immunofluorescence images of HeLa cells expressing the indicated shRNAs (maximum projections of z-stacks; scale bar: 10 μm). (B) Quantitation of Golgi fragmentation depicted in A. Non-hairpin: 16 cells; shLYSMD3 #1: 13 cells; #2: 16 cells; shFAM174B #1: 20 cells; #2: 21 cells; shZNF501: 14 cells; shZNF643: 13 cells; all data represent mean \pm SEM. ***, $p < 0.001$, ****, $p < 0.0001$ (one-way analysis of variance [ANOVA] with Tukey's multiple comparison). (C) Secretion of ssHRP over time in HeLa cells expressing the indicated shRNAs as measured by an HRP assay. Treatment with 2 μM nigericin was carried out 3 h before beginning the measurements. Data represent mean \pm SEM ($n = 2$). *, $p < 0.05$; ***, $p < 0.001$; ****, $p < 0.0001$ (one-way ANOVA with Sidak's multiple comparison). (D) Nigericin dose response measuring cell viability by CellTiter-Glo 17 h after treatment of HeLa cells expressing the indicated shRNAs. (E) Confocal microscopy images showing the localization of the indicated RFP fusion proteins (magenta) in HeLa cells expressing GA-HT2 (green). Nuclei are visualized with DAPI (blue). Top row shows low expression level and bottom row high expression level of the RFP fusion proteins (maximum projections of z-stacks; scale bar: 10 μm).

ZNF501 and ZNF643 to be localized to the nucleus, with ZNF501 enriched in nucleoli, where it could potentially be involved in transcriptional regulation (Supplemental Figure S4E). These data show

that our Golgi-specific stress system is a powerful tool that enables identification of new genes with essential roles in regulating Golgi organization.

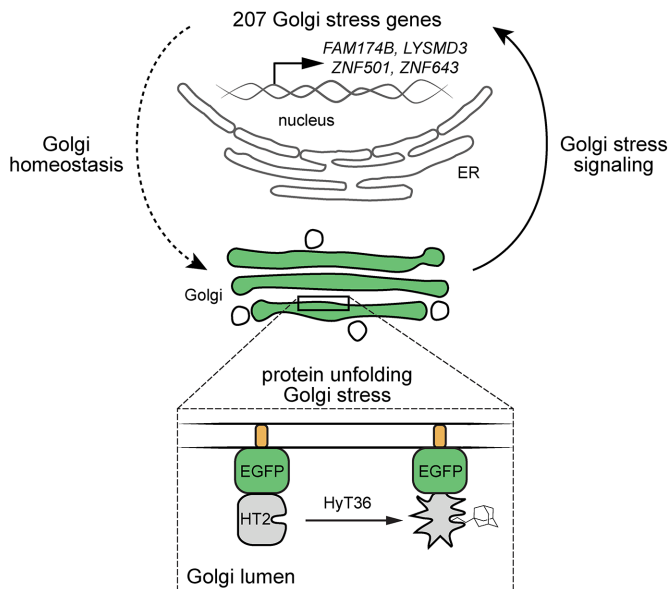


FIGURE 4: Model of Golgi stress induction. Expression of GA-HT2 and subsequent unfolding of the protein by conjugation of the hydrophobic tag HyT36 induces Golgi-specific stress. Up-regulation of Golgi stress genes, including *FAM174B*, *LYSMD3*, *ZNF501*, and *ZNF643*, is induced to restore homeostasis, illustrating a mechanism of Golgi autoregulation.

Novel insight into a Golgi-specific transcriptional stress response

In this study, we used an induced protein-unfolding system to specifically target the Golgi apparatus (Figure 4). We found that destabilization of GA-HT2 induced up-regulation of a set of Golgi-related genes whose expression is affected with similar kinetics by other stress inducers that affect the Golgi, such as nigericin and xyloside (Oku *et al.*, 2011; Taniguchi *et al.*, 2015). Importantly, these genes were not affected by HT2 destabilization in the ER, highlighting the ability of the Golgi to respond to protein-folding stress independently and indicating the presence of a Golgi-specific unfolded-protein response. The difference in kinetics between the ER and Golgi stress response appears to be a common characteristic of different types of ER and Golgi stressors. While thapsigargin, tunicamycin, and the ER-HT2 protein-unfolding system induce a response that peaks at ~2–4 h posttreatment, the transcriptional response to nigericin, monensin, and the GA-HT2 protein-unfolding system is detectable at later time points (~8–24 h) (Yoshida *et al.*, 2001; Oku *et al.*, 2011; Raina *et al.*, 2014; Baumann *et al.*, 2017). For detailed studies on Golgi stress kinetics, it will be important to identify the direct molecular signal(s) that are sensed during Golgi stress and serve as the starting point for initiating the transcriptional response. This will support defining the threshold of stress that warrants activation of the transcriptional response. The lag phase of the Golgi transcriptional stress response could be inherent to the yet-to-be-identified stress-signaling cascade, or it could relate to initial buffering of the stress by nontranscriptional aspects of the Golgi stress response. Another difference between the Golgi and ER stress responses is the generally smaller transcriptional change of genes during Golgi stress. At this point, we can only speculate about the mechanistic basis of this phenomenon, but it may reflect the nature of the Golgi, which has a smaller volume than the ER, or the nature of the transcriptional response being a late-stage cellular response to Golgi stress.

Transcriptome profiling by RNA sequencing of cells treated with the various stressors demonstrated that the GA-HT2 system affects genes associated specifically with the Golgi, while nigericin and xyloside induce broad changes. In addition to transcription, it will be important to characterize more proximal effects of Golgi stress. For instance, Src activation could alleviate Golgi stress through its control of intra-Golgi trafficking (Pulvirenti *et al.*, 2008; Giannotta *et al.*, 2012), or dephosphorylation of a Golgi structural protein like GRASP65 or GM130 could enhance Golgi stability (Nakamura *et al.*, 1997; Wang *et al.*, 2005). To this end, use of the GA-HT2 system will be especially effective, owing to the clarity provided by its reduced off-target effects relative to those of other Golgi stressors.

Previously characterized organelle-specific stress responses leverage many different strategies to restore homeostasis. So-called adaptive stress-response pathways regulate the capacity of the organelle in response to cellular needs. The ER stress response, for example, can affect ER structure and increase its capacity, increase export via ER-associated degradation or secretion, reduce import via translational down-regulation, and affect the folding capacity of the ER itself by specifically enhancing expression of protein chaperones (Hetz, 2012). The transcriptional response to Golgi stress reflects a number of potential adaptive strategies that the Golgi may use to restore homeostasis, such as by regulating vesicle-mediated transport, glycosylation, or Golgi structure. We further explored the roles of uncharacterized Golgi stress-responsive genes from our RNA-sequencing study and found that shRNA-mediated knock-down of *FAM174B*, *LYSMD3*, *ZNF501*, or *ZNF643* led to disrupted Golgi morphology, implicating them in Golgi structural regulation. The observed Golgi disruption phenotype resembles that seen in different disease states, such as in specific types of cancers (Kellokumpu *et al.*, 2002; Baschieri *et al.*, 2014, 2015; Petrosyan *et al.*, 2014). Exploring the regulation of the identified Golgi stress genes, specifically of *FAM174B*, *LYSMD3*, *ZNF501*, and *ZNF643*, in these contexts will help to further characterize the relationship between Golgi integrity and disease. Stress-response pathways are often part of the so-called nononcogenic addiction of cancer cells and have been used as the basis for development of therapeutics (Hetz *et al.*, 2013). Accordingly, the Golgi-specific stress response could serve as a potential drug target.

Despite being sensed and inducing a transcriptional response, unfolded GA-HT2 remains at steady levels even after 48 h of destabilization, in contrast to unfolded HT2 in the cytosol or ER, which is degraded by the proteasome (Neklesa *et al.*, 2011; Raina *et al.*, 2014). This suggests that destabilized Golgi proteins may be subjected to a quality-control route that does not involve protein degradation, or perhaps the level of destabilization induced by hydrophobic tagging of HT2 is insufficient to warrant activation of Golgi-related degradation pathways. Linstedt and colleagues recently demonstrated that induced oligomerization of ectopically expressed Golgi proteins leads to lysosome-mediated degradation of the oligomer (Tewari *et al.*, 2015). Thus, it is possible that the Golgi may respond differently to different degrees of protein-folding stress, with moderate protein destabilization inducing an acute stress that spares proteins from degradation and destabilization that is capable of producing aggregates inducing lysosome-mediated degradation. Our Golgi stress model is an important tool to further characterize the immediate response of the Golgi to unfolded proteins. Additionally, late-stage up-regulation of ER stress genes after hydrophobic tagging of GA-HT2 indicates that the Golgi might profit from aspects of the ER unfolded-protein response to maintain its own homeostasis.

Taken together, the developed Golgi stress model allowed us to uncover a Golgi-specific transcriptional stress response that

comprises previously uncharacterized proteins involved in regulating Golgi structure. Their knockdown induces sustained Golgi disruption, and future work will focus on their roles during Golgi stress. This novel approach to induce a Golgi-specific stress is a valuable tool for the characterization of homeostasis mechanisms used by the Golgi apparatus and will be useful for future studies addressing the Golgi's response to protein unfolding and Golgi-related protein quality-control pathways.

MATERIALS AND METHODS

Reagents

HyT36 was synthesized according to the procedure described previously (Tae *et al.*, 2012). The synthesis of HyT36(-Cl) is described below. All other compounds were obtained from the following suppliers: nigericin (EMD Millipore), xyloside (Sigma), cycloheximide (Sigma), doxycycline (Sigma), HALTS1 (ChemBridge; #9074451), TMB-Plus Substrate-Chromogen (Agilent), zeocin (Invivogen), blasticidin (Invivogen), hygromycin (Thermo Fisher Scientific), puromycin (Invivogen). Antibodies: α -HA (Cell Signaling; 3724, 1:1000), α -tubulin (Sigma; T9026, 1:10,000), α -giantin (Abcam; ab24586, 1:1000), α -LYSMD3 (Proteintech; 24313-1-AP, 1:1000).

The shRNAs used in this study are shown in Table 2.

Cell culture and generation of stable cell lines

HEK293 Flp-In T-Rex cells (Thermo Fisher Scientific), HeLa Flp-In T-Rex cells (gift from Stephen Taylor, University of Manchester), and HEK293T cells were cultured in DMEM (Thermo Fisher Scientific) supplemented with 10% fetal bovine serum (FBS; Thermo Fisher Scientific), 100 U/ml penicillin and 100 μ g/ml streptomycin (Thermo Fisher Scientific), at 37°C and 5% CO₂. Cell lines are periodically tested for mycoplasma contamination.

Stable cell lines containing a doxycycline-inducible HT2-fusion protein were generated using the Flp-In T-Rex system (Thermo Fisher Scientific) according to the manufacturer's protocol. Parental HEK293 Flp-In T-Rex and HeLa Flp-In T-Rex cells were cultured in 100 μ g/ml zeocin and 15 μ g/ml blasticidin, and 50 μ g/ml zeocin and 4 μ g/ml blasticidin, respectively. Stable cyto-HT2, ER-HT2 or GA-HT2 HEK293 and HeLa cells were selected and cultured in 100 μ g/ml hygromycin and 15 μ g/ml blasticidin, and 200 μ g/ml hygromycin and 4 μ g/ml blasticidin, respectively. Subclones were selected by isolating individual foci from 15-cm dishes.

shRNA knockdown cell lines were generated using a lentiviral system. Virus was generated in HEK293T cells by transfecting the pLKO, packaging (psPAX2), and envelope (pMD2) plasmids in a 10:10:1 ratio. Media were replenished after 12 h, and viral media were collected 48 h posttransfection and immediately transferred onto GA-HT2 HEK293 or HeLa cells in the presence of polybrene (Sigma). After 24–48 h, transduced HEK293 and HeLa were selected with 1.5 and 1 μ g/ml puromycin, respectively.

Gene	Target sequence	TRC no.
Non-hairpin	CCGCAGGTATGCACGCGT	n/a
LYSMD3#1	ATTCTTACATAGGCTATATA	TRCN0000253829
LYSMD3#2	GAACCTCAATGAGGTAGTATC	TRCN0000253830
FAM174B#1	CCACAGTATTCGACATCAAAT	TRCN0000116173
FAM174B#2	CACAGTATTCGACATCAAATA	TRCN0000116174
ZNF501	CCCTGACATTAAGTGAATAAA	TRCN0000107850
ZNF643	GCCAGAGAATACATCTTTCTA	TRCN0000016540

TABLE 2: shRNAs used.

For experiments involving HT2 destabilization, cells were first treated with 100 ng/ml doxycycline (Sigma) for 16–24 h before treatment with 10 μ M HyT36 or HyT36(-Cl) for indicated times in the presence of doxycycline. HALTS1 treatments were performed at 10 μ M concurrently with doxycycline treatment. The 1 μ M nigericin (EMD Millipore) and 4 mM xyloside (Sigma) treatments were performed in the absence of doxycycline for the indicated times. Co-treatments with 20 μ g/ml cycloheximide (Sigma) were performed for the final 8 h of the treatments described above. DNA transfections were performed using Lipofectamine 2000 Transfection Reagent (Thermo Fisher Scientific) according to the manufacturer's protocol. For transient transfection of RFP fusion proteins, 200 ng DNA per well of a six-well plate was used.

Cloning

The GA-HT2 construct was created with the USER cloning strategy (Nour-Eldin *et al.*, 2010). Briefly, the DNA fragments of interest were PCR amplified with uracil-containing primers using PfuTurbo Cx Hotstart DNA Polymerase (Agilent Technologies) according to the manufacturer's protocol. Purified fragments were combined in a three-part assembly reaction using the USER Enzyme and DpnI (New England Biolabs). The fragments included the first 61 amino acids from B4GALT1 corresponding to its transmembrane domain, HA-EGFP-HT2 hemagglutinin-tag enhanced green fluorescent protein obtained from previously described constructs (Neklesa *et al.*, 2011; Raina *et al.*, 2014), and pcDNA5/FRT/TO (Thermo Fisher Scientific). For the described construct, the HA-EGFP-HT2 moiety faces the Golgi lumen. All other constructs were prepared with restriction enzyme-based cloning. Luciferase-HT2 (firefly luciferase-HA-HT2) was cloned from a previously described construct (Neklesa *et al.*, 2011) into pET21a. ER-HT2 (Calreticulin(SS)-HA-EGFP-HT2-KDEL) and cyto-HT2 (HA-EGFP-HT2) were cloned from previously described constructs into pcDNA5/FRT/TO (Neklesa *et al.*, 2011; Raina *et al.*, 2014). These constructs are expressed as soluble proteins in the ER and the cytosol, respectively. FAM174B, LYSMD3, ZNF501, and ZNF643 were cloned from HEK293 cDNA. RNA was extracted as described in the section *RNA extraction and qPCR*, and cDNA was prepared with the Agilent AffinityScript cDNA Synthesis Kit according to the manufacturer's instructions. Obtained PCR products were digested and ligated into pcDNA3 already containing FLAG-mRFP or mRFP-FLAG in front of or after the multiple cloning site for generating C-terminal and N-terminal fusion proteins, respectively. A plasmid containing the signal sequence of HGH1 fused to horseradish peroxidase (HRP), referred to as ssHRP, was a gift from the Rothman lab, Yale University (Connolly *et al.*, 1994).

Cell viability determination using CellTiter-Glo

HeLa cells were plated at a density of 750 cells/well in a 384-well plate. The following day, cells were treated by addition of 6x stocks of nigericin in culture medium to reach the final concentrations indicated in Figure 3D. After 17 h of incubation, cell viability was measured using the CellTiter-Glo Luminescent Cell Viability Assay (Promega; G7572) according to the manufacturer's instructions.

HRP secretion assay

Cells were transiently transfected with the ssHRP plasmid. After 24–48 h of transfection and appropriate treatment, cells were washed twice with culture media. Subsequently, aliquots of media (80 μ l from 2 ml) were collected at 0, 1, and 2 h postwash. After the last time point, cells were washed twice in phosphate-buffered saline (PBS) and lysed in 50 mM Tris (pH 8.0), 150 mM NaCl, 1% NP-40, and 1x Roche EDTA-free Complete Protease Inhibitor Cocktail. Media and lysate

samples were cleared by centrifugation at $500 \times g$ for 5 min. Fifteen microliters of each sample was mixed with 30 μ l of TMB reagent and incubated for 15–60 min. The reaction was stopped by adding 30 μ l 1 N H_2SO_4 , and absorbance at 450 nm was measured on a Wallac Victor 2 Plate Reader (Perkin Elmer). For data analysis, the levels of ssHRP detected in the media were subtracted from the level at 0 h and then normalized to the level of ssHRP detected in the cell lysate.

Protein expression and purification

Luciferase-HT2 in pET21a was overexpressed in BL21(DE3) cells. Protein expression was induced with 250 μ M isopropyl β -D-1-thiogalactopyranoside for 5 h at 25°C. Cells were harvested by centrifugation, resuspended in lysis buffer containing 50 mM Na_2HPO_4 (pH 8.0), 300 mM NaCl, and lysed by sonication. Cleared cell lysate was incubated with NiNTA agarose beads (Qiagen). After 60 min of incubation, the beads were washed by applying a stepwise imidazole gradient and the luciferase-HT2 protein was finally eluted using 150 mM imidazole in lysis buffer. Subsequently, the protein was subjected to size-exclusion chromatography using a Superdex 200 column (GE Healthcare) equilibrated with 50 mM HEPES (pH 7.5), 150 mM NaCl.

In vitro luciferase assays

For luciferase assays, 1 μ M luciferase-HT2-His₆ was incubated with 10 μ M HyT36, HyT36(-Cl), or dimethyl sulfoxide (DMSO) for 30 min at room temperature. Reactions were transferred to a 96-well plate, and luciferase activity was measured on a Wallac Victor 2 Plate Reader (Perkin Elmer). A reaction mix of 1 mM D-luciferin, 1 mM ATP, 50 μ M CoA in 20 mM potassium phosphate (pH 7.8), 15 mM $MgSO_4$, 4 mM ethylene-bis(oxyethylenitrilo)tetraacetic acid, and 1 mM dithiothreitol was added to each well, and luminescence was measured. Reactions were performed in triplicate, and data were normalized to DMSO control.

Cell counting

Cultured cells were trypsinized and resuspended in DMEM. Cell counting was done using a Bio-Rad TC20 automated cell counter according to the manufacturer's protocol.

Confocal microscopy and image analysis

For microscopy experiments cells were grown on coverslips and, after the indicated treatment, fixed in 4% paraformaldehyde in PBS. For giantin immunofluorescence, cells were permeabilized, and blocked in 10% FBS in PBS + 0.01% Triton X-100, incubated with α -giantin primary antibody diluted in 3% BSA in PBS + 0.01% Triton X-100 for 60 min at room temperature and α -rabbit secondary antibody conjugated to Alexa Fluor 633 (Thermo Fisher) diluted 1:500 in 3% BSA in PBS + 0.01% Triton X-100 for 60 min at room temperature. Coverslips were mounted on microscopy slides in Vectashield mounting medium (Vector Laboratories). Images were acquired on a Zeiss LSM 880. Z-stacks (1- μ m slices) spanning the entire volume of the cells were recorded with oil-immersion 40 \times and 63 \times Plan-Apochromat lenses, 1.3 and 1.4 NA, respectively. Images were processed using Fiji (Schindelin et al., 2012).

Electron microscopy

Cultured cells were fixed in 2.5% glutaraldehyde in 0.1 M sodium cacodylate buffer (pH 7.4) at room temperature for 1 h, and then they were scraped off and pelleted in 2% agar. Cells were further postfixed in 1% OsO_4 at room temperature for 30 min, followed by another 30 min in 1% tannic acid solution. They were stained en bloc with 2% aqueous uranyl acetate for 15 min, dehydrated in a graded

series of ethanol to 100%, propylene oxide, and embedded in EMBED 812 resin (Electron Microscopy Sciences). Blocks were polymerized at 60°C for 24 h. Thin sections (60 nm) were cut by a Leica ultramicrotome and poststained with 2% uranyl acetate and lead citrate. Sample sections were examined in a Tecnai Biotwin transmission electron microscope (FEI) at 80 kV of the accelerating voltage; digital images were acquired by an Olympus Morada CCD camera and iTEM imaging software. EM experiments were performed by the Center for Cellular and Molecular Imaging at Yale University.

Preparation of cell lysates and Western blotting

Cultured cells were washed with PBS (Thermo Fisher Scientific) and resuspended in RIPA lysis buffer (50 mM Tris, pH 7.5, 150 mM NaCl, 1% NP-40, 0.1% SDS, 0.5% sodium deoxycholate, 1 mM EDTA, 1 \times Roche EDTA-free Complete Protease Inhibitor Cocktail). Protein concentrations were determined by bicinchoninic acid (BCA) assay (Thermo Fisher Scientific), and 20–60 μ g total protein per sample was loaded on an SDS-PAGE gel. Western blotting followed using standard protocols.

Limited proteolysis of cell lysates

Cultured cells, treated with DMSO, HyT36, or HyT36(-Cl) for 12 h, were washed with PBS and lysed in 50 mM Tris (pH 7.5), 150 mM NaCl, 1 mM EDTA, 0.1% NP-40. The soluble fraction of the cell lysate was diluted to 2 mg/ml as determined by a BCA assay (Thermo Fisher Scientific). Upon addition of the indicated amount of trypsin (Sigma), reactions were incubated for 5 min on ice. Reactions were stopped by adding SDS-PAGE sample buffer and boiling. Samples were resolved on SDS-PAGE gels and analyzed by Western blotting.

Flow cytometry

Cultured cells were trypsinized and resuspended in DMEM to $\sim 1 \times 10^6$ cells/ml. Cellular GFP fluorescence was measured on a BD FACSCalibur (BD Biosciences). Data were analyzed using BD CellQuest Pro software.

RNA extraction and qPCR

Cultured cells were resuspended in Trizol (Thermo Fisher Scientific) for RNA extraction (0.5 ml Trizol for 12-well plate or 1 ml Trizol for six-well plate). One part chloroform was added to five parts Trizol and samples were vortexed and spun at $12,000 \times g$ for 15 min at 4°C. The top phase was recovered, and one part was mixed with 1–1.5 parts isopropanol. After a 10-min incubation, samples were spun at $12,000 \times g$ for 10 min at 4°C. The supernatant was decanted, and the pellet was washed twice with 75% ethanol. RNA pellets were dried and resuspended in nuclease-free water. cDNA was synthesized using the High Capacity cDNA Reverse Transcription Kit (Thermo Fisher Scientific). Real-time qPCR was performed using FastStart Universal SYBR Green Master (ROX) (Roche) on a LightCycler 480 II (Roche), with 40 cycles of 15 s at 95°C and 45 s at 60°C. Transcripts were normalized to the housekeeping gene *ACTB*, and all measurements were performed in duplicate. For primer sequences, see Table 3. Data were analyzed with LightCycler 480 software and statistics were calculated with Prism (GraphPad).

RNA sequencing and data analysis

Cells were treated for 12 h in biological duplicate with DMSO and 10 μ M HyT36 in the presence of 100 ng/ml doxycycline, and with DMSO, 10 μ M HyT36, 1 μ M nigericin, or 4 mM xyloside in the absence of doxycycline at 37°C. Cells were harvested, and RNA was extracted using the RNeasy Mini Kit (Qiagen) according to the manufacturer's instructions. Total RNA was quantified using a NanoDrop (ND-1000).

Gene	Forward primer	Reverse primer
ACTB	GAGAAGAGCTACGAGCTGCCTGAC	ACTGTGTTGGCGTACAGGTCTTTG
PCSK1	GGACCTCTGAGTATGACCCG	AGCTTTGGCATTAGCAAGCC
STX3A	TCGGCAGACCTTCGGATTC	TCCTCATCGGTTGTCTTTTTGC
GM130	ACGCCCTCAGGCTGGAGTTA	GAAGCAGGAGTCCGTCATCTCTA
GOLGB1	CACTCAGGAGCAGGCACTGTTA	CAGGACTCGCTTCCATCCAA
WIPI49	AGTCAGTCACACAAAACACG	AGAGCACATAGACCTGTTGGG
FUT1	TGGACTGTCTACCCCAATGG	CAGGGTGATGCGGAATACCG
GCP60	AGCGTGCATGTCAGTGAGTCC	GGCACAATCTCATCCAGCAAAG
UAP1L1	CCAACGTGGTCATGTTTGAGC	GGATGTTGTCCACACAGTACAC
SIAT4A	GGAGGACGACACCTACCGAT	CCACCGACCTCTTCTCCAG
LYSMD3	ATGAGGTAGTATCGGCCTTAACA	GTCTGCTCCATAATAGGGGTCT
FAM174B	CCTTGGTGACCCGCATTTT	GTAAGGCGAACGCCACGA
ZNF501	AACTTTCCGCAAACAAGCACA	TCCCACATCCAACACTCATA
ZNF643	GCAGCATGTATTCCACCTTGG	CCCCTTACCATTCTTTGGTTC
CHOP	GAACGGCTCAAGCAGGAAATC	TTCACCATTGCGTCAATCAGAG
ERDJ4	TGGTGGTCCAGTAGACAAAGG	CTTCGTTGAGTGACAGTCTGTC

TABLE 3: Primers used for qPCR.

Twelve strand-specific sequencing libraries, two replicates per condition, were produced from the total RNA. Total mRNA was purified from ~500 ng of total RNA with Ribo-Zero and sheared by incubation at 94°C. cDNA libraries underwent 76–base pair single-end sequencing on an Illumina HiSeq 2500, according to Illumina protocols, generating between 22M and 31M reads per library. RNA sequencing was performed by the Yale Center for Genome Analysis.

The first six nucleotides and the last nucleotides with a quality score below 20 for each read were trimmed using in-house scripts. If, after trimming, the read was shorter than 45 base pairs, the whole read was discarded. Trimmed reads were mapped to the human reference genome (hg19) with a known transcriptome index (UCSC Known Gene annotation) using Tophat version 2.0.13 (Trapnell *et al.*, 2009). Only the reads that mapped to a single unique location within the genome, with a maximum of two mismatches in the anchor region of the spliced alignment, were reported in these results. Tophat alignments were then processed by Cufflinks version 2.2.1 (Trapnell *et al.*, 2010) to obtain differential gene expression. The HyT36 data set was further processed to control for off-target effects of HyT36. The fold changes of genes affected between DMSO and HyT36 in the presence of doxycycline were normalized to their fold changes in the absence of doxycycline, provided the changes in both comparisons had a false discovery rate–adjusted *p* value of less than 0.05. The adjusted list was subsequently processed in Ingenuity Pathway Analysis (Qiagen) in parallel to the comparisons between DMSO and nigericin or xyloside to generate the final data sets (Supplemental Table S1). Gene Ontology analysis was performed with HOMER version 4.7 (Heinz *et al.*, 2010).

Statistical analysis and data reproducibility

Statistical tests and *p* values are described in the figure legends. Sample sizes were determined empirically to give reproducible conclusions between multiple independent experiments. Limited proteolysis was performed in technical duplicates. Flow cytometry was performed in biological duplicates. Cell counting was performed in biological triplicates, and statistics were calculated from the average of technical duplicates. qPCR experiments were performed in bio-

logical duplicates, and statistics were calculated from the average of technical duplicates.

Golgi compactness was quantified as previously described (Bard *et al.*, 2003). Briefly, maximum projections of z-stacks were generated and background pixels were removed by setting the minimum threshold to 90 on a black-and-white image scale (0–250). A region of interest was drawn around the Golgi, and the area and perimeter of the Golgi particles contained was determined (minimum area of 3 pixels²). Compactness was calculated with the formula $4\pi(\text{sum}(\text{areas})/[\text{sum}(\text{perimeters})]^2)$. Statistics were calculated with Prism (GraphPad). Golgi compactness was calculated from at least 13 individual cells in a single experiment.

Experiments were reproduced multiple independent times. Specifically, colocalization between GA-HT2 and giantin was performed more than 10 times. Limited proteolysis was performed twice. Western blotting for GA-HT2 in response to HyT36 treatment was performed more than five times. qPCR analysis of Golgi stress genes was performed more than 10 times in HEK293 cells and twice in HeLa cells. Golgi- and ER-stress kinetic analysis by qPCR was performed twice. RNA sequencing was performed once. Giantin immunofluorescence in Golgi stress gene-knockdown cell lines was performed three times. ssHRP secretion in HeLa and HEK293 cell lines was performed once. The nigericin dose–response assay in HeLa cells was performed twice. In vitro luciferase assays were performed more than 5 times in HEK293 cells and twice in HeLa cells. The HEK293 toxicity assay was performed twice. EM analysis of GA-HT2–expressing HeLa cells was performed twice. qPCR of HEK293 cells subjected to varying concentrations of doxycycline was performed twice. Analysis of LYSMD3 protein levels by Western blotting was performed twice. EM analysis of Golgi stress gene-knockdown cell lines was performed once. Imaging of RFP-fused Golgi stress genes was performed twice.

Data availability

RNA-sequencing data were deposited in the NCBI GEO database (GSE99490).

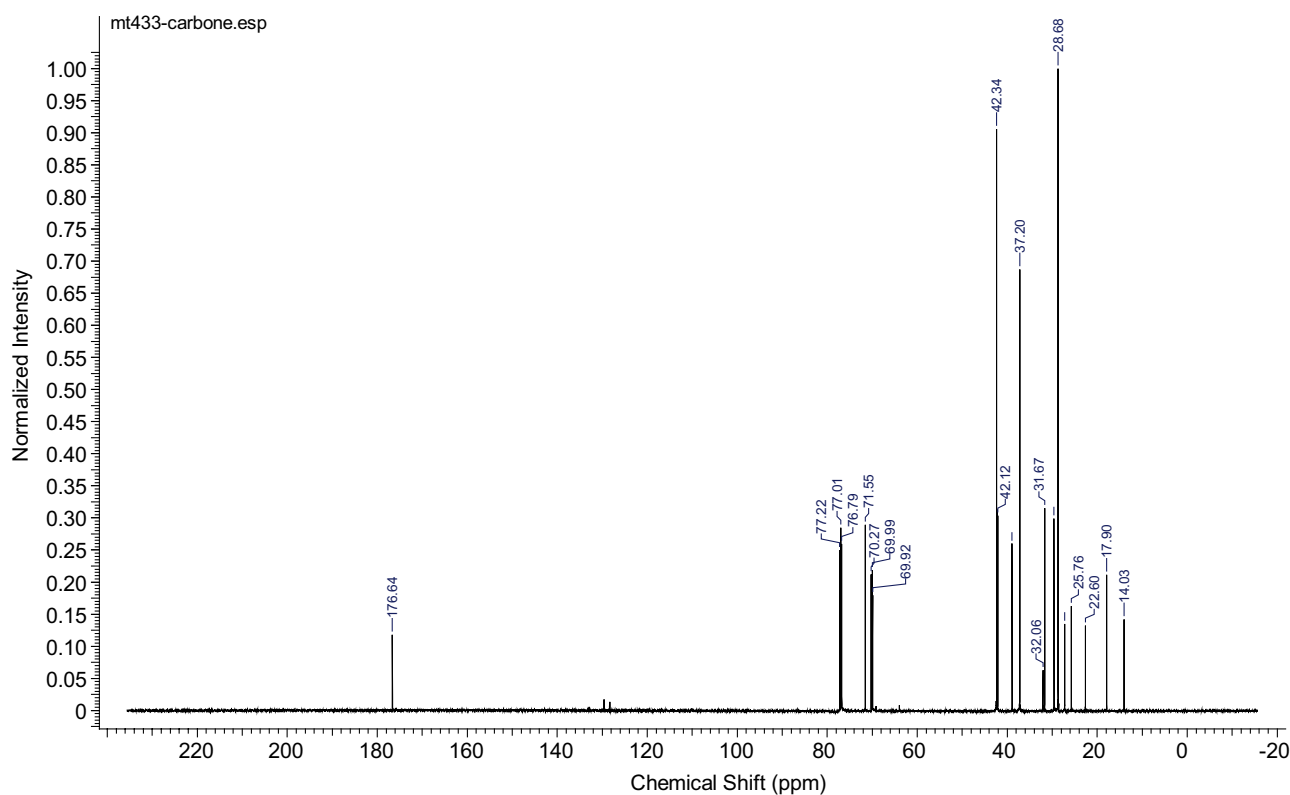
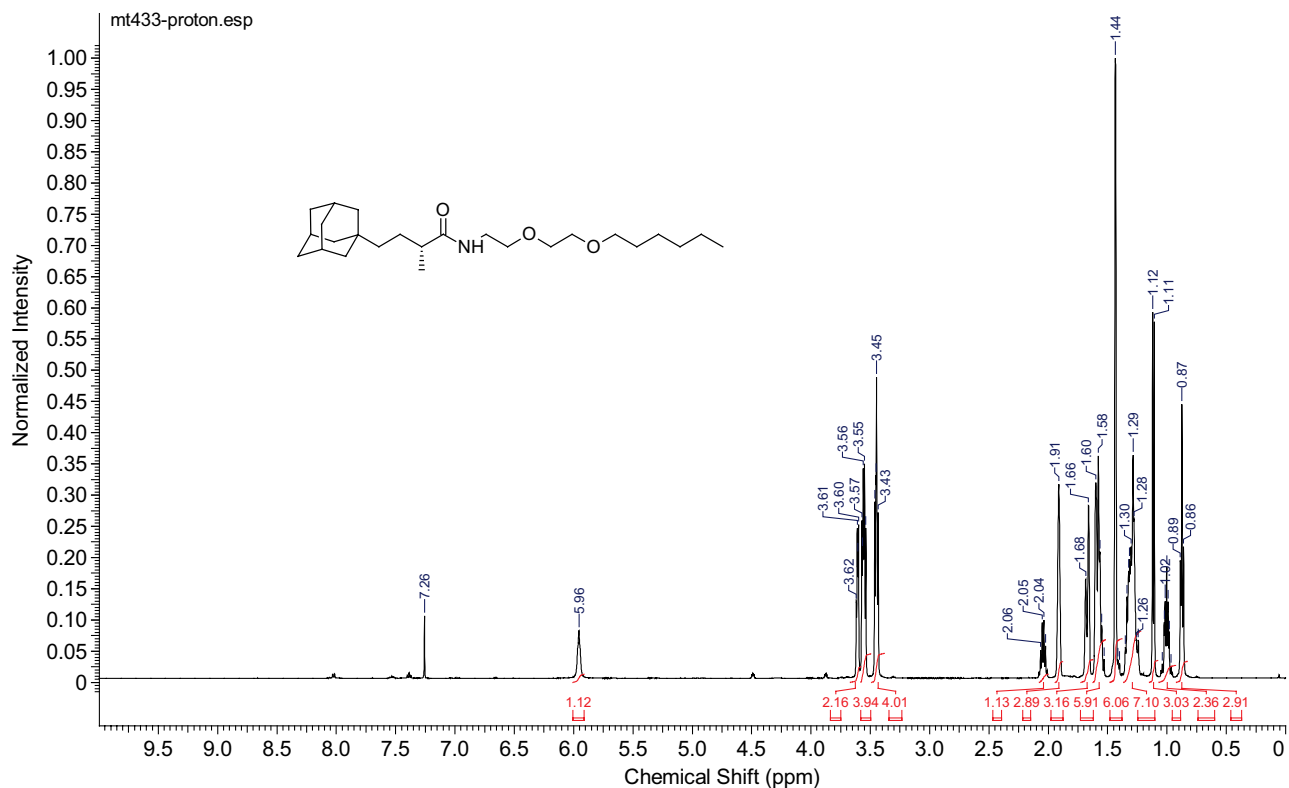


FIGURE 5: NMR spectra.

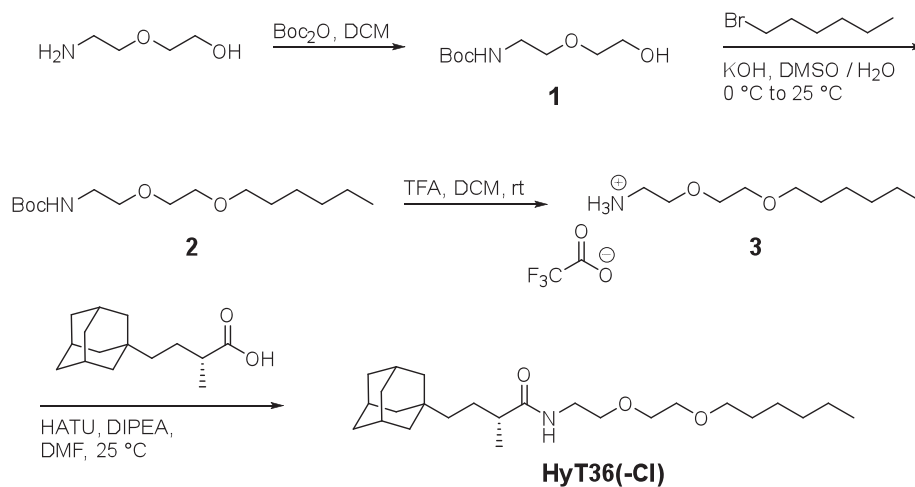
Synthesis of HyT36(-Cl)

Unless otherwise indicated, common reagents or materials were obtained from commercial sources and used without further purification. Tetrahydrofuran (THF) and dichloromethane (CH_2Cl_2) were dried by a PureSolv solvent-drying system. Flash column

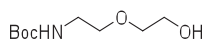
chromatography was performed using silica gel 60 (230–400 mesh). Analytical thin-layer chromatography was carried out on Merck silica gel plates with QF-254 indicator and visualized by UV or KMnO_4 . ^1H and ^{13}C NMR spectra (Figure 5) were recorded on an Agilent DD₂ 500 (500 MHz ^1H ; 125 MHz ^{13}C) or Agilent

DD₂ 600 (600 MHz ¹H; 150 MHz ¹³C) or Agilent DD₂ 400 (400 MHz ¹H; 100 MHz ¹³C) spectrometer at room temperature. Chemical shifts were reported in parts per million relative to the residual CDCl₃ (δ 7.26 ppm ¹H; δ 77.00 ppm ¹³C), CD₃OD (δ 3.31 ppm ¹H; δ 49.00 ppm ¹³C), or d⁶-DMSO (δ 2.50 ppm ¹H; δ 39.52 ppm ¹³C). NMR chemical shifts were expressed in parts per million relative to internal solvent peaks, and coupling constants were measured in hertz (bs = broad signal). Mass spectra were obtained using electrospray ionization (ESI) on a time-of-flight mass spectrometer.

Synthesis scheme of HyT36(-Cl)



tert-Butyl (2-(2-hydroxyethoxy)ethyl)carbamate (**1**).



To a solution of 2-(2-aminoethoxy)ethanol (4.74 ml, 47.56 mmol) in anhydrous THF (100 ml) was added BOC anhydride (10.38 g, 0.05 mol) at 0°C. After being stirred at room temperature for 2 h, the solvent was removed under reduced pressure. The product was dissolved in CH₂Cl₂ (100 ml), then water (100 ml) was added. The layers were separated and the aqueous phase was extracted with CH₂Cl₂ (2 × 100 ml). The combined organic layers were dried over Na₂SO₄, filtered, and evaporated under vacuum to obtain the product, 9.6 g (99%) of **1**, which was used in the next step without further purification. NMR data are in accordance with the literature.

¹H NMR (500 MHz, Chloroform-*d*) δ 5.07 (bs, 1H), 3.72 (d, *J* = 4.1 Hz, 2H), 3.55 (d, *J* = 16.3 Hz, 4H), 3.32 (s, 2H), 2.59 (s, 1H), 1.43 (s, 9H).

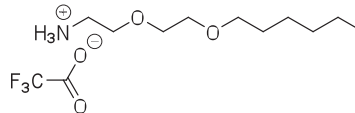
tert-Butyl (2-(2-(hexyloxy)ethoxy)ethyl)carbamate (**2**).

A solution of **1** (1.01 g, 4.9 mmol) and KOH (277.2 mg, 5.0 mmol) in DMSO (50 ml) and distilled water (5 ml) was stirred 15 min at room temperature. Then the mixture was cooled to 0°C, and 1-bromohexane (0.69 ml, 4.94 mmol) was added dropwise over 1 h. The resulting solution was stirred for 1 h at 0°C and then for 8 h at room temperature. After being diluted with ethyl acetate (250 ml) and water (250 ml), the aqueous phase was extracted with ethyl acetate (3 × 100 ml). The combined organic phases were washed with brine and dried over MgSO₄ and filtered. After concentration, the crude material was subjected to column chromatography on silica gel (ethyl acetate:hexane [1:4])

to give 517 mg (36%) of **2** as a colorless oil. NMR data are in accordance with the literature.

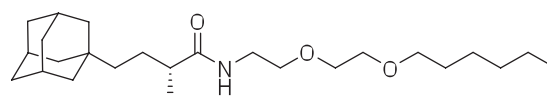
¹H NMR (500 MHz, Chloroform-*d*) δ 5.03 (s, 1H), 3.59 (dd, *J* = 6.4, 3.5 Hz, 2H), 3.56 – 3.49 (m, 4H), 3.44 (t, *J* = 6.8 Hz, 2H), 3.33 – 3.23 (m, 2H), 1.56 (dq, *J* = 13.2, 6.6 Hz, 2H), 1.42 (s, 9H), 1.37 – 1.22 (m, 6H), 0.87 (t, *J* = 6.8 Hz, 3H).

2-(2-(Hexyloxy)ethoxy)ethan-1-aminium 2,2,2-trifluoroacetate (**3**).



A solution of **2** (500 mg, 1.73 mmol) in TFA:CH₂Cl₂ (1:1) mixture was stirred at room temperature for 4 h. The solvent was evaporated to give 495 mg (100%) of **3** as a yellow oil that was carried to the next step without further purification or characterization.

(*R*)-4-((3*R*,5*R*,7*R*)-Adamantan-1-yl)-*N*-(2-(2-(hexyloxy)ethoxy)ethyl)-2-methylbutanamide (**HyT36(-Cl)**).



To a solution of **3** (15 mg, 0.06 mmol) in DMF (1 ml) was added HATU (1-[Bis(dimethylamino)methylene]-1*H*-1,2,3-triazolo[4,5-*b*]pyridinium 3-oxid hexafluorophosphate) (48.26 mg, 0.13 mmol), and the resulting solution was stirred for 10 min at room temperature, after which (2-(2-hexyloxyethoxy)ethanamine (18.17 mg, 0.06 mmol) and DIPEA (0.05 ml, 0.32 mmol) were added, respectively. The resulting mixture was stirred at room temperature for 16 h. The product was extracted twice with ethyl acetate and water. Then the combined organic phases were concentrated and the residue purified by silica gel chromatography (ethyl acetate:hexane [1:4]) to give 21 mg (82%) of **HyT36(-Cl)**.

¹H NMR (500 MHz, Chloroform-*d*) δ 5.96 (bs, 1H), 3.64 – 3.58 (m, 2H), 3.55 (dd, *J* = 11.2, 5.5 Hz, 4H), 3.49 – 3.40 (m, 4H), 2.04 (q, *J* = 6.9 Hz, 1H), 1.91 (s, 3H), 1.67 (d, *J* = 12.0 Hz, 3H), 1.57 (dd, *J* = 15.7, 9.2 Hz, 6H), 1.43 (s, 6H), 1.36 – 1.23 (m, 7H), 1.11 (d, *J* = 6.8 Hz, 3H), 1.00 (dt, *J* = 10.6, 4.2 Hz, 2H), 0.87 (t, *J* = 6.7 Hz, 3H).

¹³C NMR (151 MHz, CDCl₃) δ 176.64, 71.55, 70.27, 69.98, 69.93, 42.34, 42.25, 42.12, 38.91, 37.20, 32.06, 31.67, 29.60, 28.68, 27.25, 25.76, 22.60, 17.90, 14.03.

LC/MS (ESI); m/z [M+H]⁺ for C₂₅H₄₆NO₃, Calculated. 408.6. Found. 408.2.

ACKNOWLEDGMENTS

We thank Stephen Taylor for providing Flp-In T-REx HeLa cells and James Rothman and his lab members for helpful discussion. This work was supported by National Institutes of Health R35CA197589 and an EMBO Long-Term Fellowship to D.H. 1102-2014. Y.V.S. was supported in part by National Institutes of Health 5T32GM06754 3-12.

REFERENCES

- Bard F, Mazelin L, Péchoux-Longin C, Malhotra V, Jurdic P (2003). Src regulates Golgi structure and KDEL receptor-dependent retrograde transport to the endoplasmic reticulum. *J Biol Chem* 278, 46601–46606.
- Barinaga-Rementeria Ramirez I, Lowe M (2009). Golgins and GRASPs: holding the Golgi together. *Semin Cell Dev Biol* 20, 770–779.
- Baschieri F, Confalonieri S, Bertalot G, Di Fiore PP, Dietmaier W, Leist M, Crespo P, Macara IG, Farhan H (2014). Spatial control of Cdc42 signaling by a GM130-RasGRF complex regulates polarity and tumorigenesis. *Nat Commun* 5, 4839.
- Baschieri F, Uetz-von Allmen E, Legler DF, Farhan H (2015). Loss of GM130 in breast cancer cells and its effects on cell migration, invasion and polarity. *Cell Cycle* 14, 1139–1147.
- Baumann J, Ignashkova TI, Chirasani SR, Ramirez-Peinado S, Alborzina H, Gendarme M, Kuhnigk K, Kramer V, Lindemann RK, Reiling JH (2017). Golgi stress-induced transcriptional changes mediated by MAPK signaling and three ETS transcription factors regulate MCL1 splicing. *Mol Biol Cell* 29, 42–52.
- Bejarano E, Cabrera M, Vega L, Hidalgo J, Velasco A (2006). Golgi structural stability and biogenesis depend on associated PKA activity. *J Cell Sci* 119, 3764–3775.
- Bexiga MG, Simpson JC (2013). Human diseases associated with form and function of the Golgi complex. *Int J Mol Sci* 14, 18670–18681.
- Bierring F (1962). Electron microscopic observations on the mucus production in human and rat intestinal goblet cells. *Acta Pathol Microbiol Scand* 54, 241–252.
- Brandizzi F, Barlowe C (2013). Organization of the ER-Golgi interface for membrane traffic control. *Nat Rev Mol Cell Biol* 14, 382–392.
- Cabrera M, Muñoz M, Hidalgo J, Vega L, Martín ME, Velasco A (2003). The retrieval function of the KDEL receptor requires PKA phosphorylation of its C-terminus. *Mol Biol Cell* 14, 4114–4125.
- Connolly CN, Futter CE, Gibson A, Hopkins CR, Cutler DF (1994). Transport into and out of the Golgi complex studied by transfecting cells with cDNAs encoding horseradish peroxidase. *J Cell Biol* 127, 641–652.
- Cordeiro D, Barretta ML, Cervigni RI, Colanzi A (2012). Golgi complex fragmentation in G2/M transition: an organelle-based cell-cycle checkpoint. *IUBMB Life* 64, 661–670.
- De Matteis MA, Luini A (2008). Exiting the Golgi complex. *Nat Rev Mol Cell Biol* 9, 273–284.
- Diao A, Rahman D, Pappin DJC, Lucocq J, Lowe M (2003). The coiled-coil membrane protein golgin-84 is a novel rab effector required for Golgi ribbon formation. *J Cell Biol* 160, 201–212.
- Dinter A, Berger EG (1998). Golgi-disturbing agents. *Histochem Cell Biol* 109, 571–590.
- Encell LP, Friedman Ohana R, Zimmerman K, Otto P, Vidugiris G, Wood MG, Los GV, McDougall MG, Zimprich C, Karassina N, et al. (2012). Development of a dehalogenase-based protein fusion tag capable of rapid, selective and covalent attachment to customizable ligands. *Curr Chem Genomics* 6, 55–71.
- Farhan H, Rabouille C (2011). Signalling to and from the secretory pathway. *J Cell Sci* 124, 171–180.
- Freeze HH, Sampath D, Varki A (1993). Alpha- and beta-xylosides alter glycolipid synthesis in human melanoma and Chinese hamster ovary cells. *J Biol Chem* 268, 1618–1627.
- Giannotta M, Ruggiero C, Grossi M, Cancino J, Capitani M, Pulvirenti T, Consoli GM, Geraci C, Fanelli F, Luini A, et al. (2012). The KDEL receptor couples to Gαq/11 to activate Src kinases and regulate transport through the Golgi. *EMBO J* 31, 2869–2881.
- Hamati HF, Britton EL, Carey DJ (1989). Inhibition of proteoglycan synthesis alters extracellular matrix deposition, proliferation, and cytoskeletal organization of rat aortic smooth muscle cells in culture. *J Cell Biol* 108, 2495–2505.
- Heinz S, Benner C, Spann N, Bertolino E, Lin YC, Laslo P, Cheng JX, Murre C, Singh H, Glass CK (2010). Simple combinations of lineage-determining transcription factors prime cis-regulatory elements required for macrophage and B cell identities. *Mol Cell* 38, 576–589.
- Hetz C (2012). The unfolded protein response: controlling cell fate decisions under ER stress and beyond. *Nat Rev Mol Cell Biol* 13, 89–102.
- Hetz C, Chevet E, Harding HP (2013). Targeting the unfolded protein response in disease. *Nat Rev Drug Discov* 12, 703–719.
- Jiang Q, Wang L, Guan Y, Xu H, Niu Y, Han L, Wei YP, Lin L, Chu J, Wang Q, et al. (2014). Golgin-84-associated Golgi fragmentation triggers tau hyperphosphorylation by activation of cyclin-dependent kinase-5 and extracellular signal-regulated kinase. *Neurobiol Aging* 35, 1352–1363.
- Joshi G, Chi Y, Huang Z, Wang Y (2014). Aβ-induced Golgi fragmentation in Alzheimer's disease enhances Aβ production. *Proc Natl Acad Sci USA* 111, E1230–E1239.
- Kellokumpu S, Sormunen R, Kellokumpu I (2002). Abnormal glycosylation and altered Golgi structure in colorectal cancer: dependence on intracellular pH. *FEBS Lett* 516, 217–224.
- Lippincott-Schwartz J, Phair RD (2010). Lipids and cholesterol as regulators of traffic in the endomembrane system. *Annu Rev Biophys* 39, 559–578.
- Los GV, Encell LP, McDougall MG, Hartzell DD, Karassina N, Zimprich C, Wood MG, Learish R, Ohana RF, Uhr M, et al. (2008). HaloTag: a novel protein labeling technology for cell imaging and protein analysis. *ACS Chem Biol* 3, 373–382.
- Makowski SL, Tran TT, Field SJ (2017). Emerging themes of regulation at the Golgi. *Curr Opin Cell Biol* 45, 17–23.
- Martin ME, Hidalgo J, Rosa JL, Crottet P, Velasco A (2000). Effect of protein kinase A activity on the association of ADP-ribosylation factor 1 to Golgi membranes. *J Biol Chem* 275, 19050–19059.
- Mavillard F, Hidalgo J, Megias D, Levitsky KL, Velasco A (2010). PKA-mediated Golgi remodeling during cAMP signal transmission. *Traffic* 11, 90–109.
- Mayinger P (2011). Signaling at the Golgi. *Cold Spring Harb Perspect Biol* 3, 1–14.
- Miyata S, Mizuno T, Koyama Y, Katayama T, Tohyama M (2013). The endoplasmic reticulum-resident chaperone heat shock protein 47 protects the Golgi apparatus from the effects of O-glycosylation inhibition. *PLoS One* 8, e69732.
- Mollenhauer HH, Morré DJ, Rowe LD (1990). Alteration of intracellular traffic by monensin; mechanism, specificity and relationship to toxicity. *Biochim Biophys Acta* 1031, 225–246.
- Moreno KW, Tiemeyer M, Nairn AV (2012). Vertebrate protein glycosylation: diversity, synthesis and function. *Nat Rev Mol Cell Biol* 13, 448–462.
- Morre JD, Mollenhauer HH (2009). *The Golgi Apparatus*, New York: Springer.
- Muñoz M, Martín ME, Hidalgo J, Velasco A (1997). Protein kinase A activity is required for the budding of constitutive transport vesicles from the trans-Golgi network. *Proc Natl Acad Sci USA* 94, 14461–14466.
- Nakamura N, Lowe M, Levine TP, Rabouille C, Warren G (1997). The vesicle docking protein p115 binds GM130, a cis-Golgi matrix protein, in a mitotically regulated manner. *Cell* 89, 445–455.
- Neklesa TK, Noblin DJ, Kuzin A, Lew S, Seetharaman J, Acton TB, Kornhaber G, Xiao R, Montelione GT, Tong L, et al. (2013). A bidirectional system for the dynamic small molecule control of intracellular fusion proteins. *ACS Chem Biol* 8, 2293–2300.
- Neklesa TK, Tae HS, Schneekloth AR, Stulberg MJ, Corson TW, Sundberg TB, Raina K, Holley SA, Crews CM (2011). Small-molecule hydrophobic tagging-induced degradation of HaloTag fusion proteins. *Nat Chem Biol* 7, 538–543.
- Nour-Eldin HH, Geu-Flores F, Halkier BA (2010). USER cloning and USER fusion: the ideal cloning techniques for small and big laboratories. *Methods Mol Biol* 643, 185–200.
- Okayama M, Kimata K, Suzuki S (1973). The influence of p-nitrophenyl beta-D-xyloside on the synthesis of proteochondroitin sulfate by slices of embryonic chick cartilage. *J Biochem* 74, 1069–1073.
- Oku M, Tanakura S, Uemura A, Sohma M, Misumi Y, Taniguchi M, Wabayashi S, Yoshida H (2011). Novel cis-acting element GASE regulates transcriptional induction by the Golgi stress response. *Cell Struct Funct* 36, 1–12.
- Petrosyan A, Holzapfel MS, Muirhead DE, Cheng P-W (2014). Restoration of compact Golgi morphology in advanced prostate cancer enhances susceptibility to galectin-1-induced apoptosis by modifying mucin O-glycan synthesis. *Mol Cancer Res* 12, 1704–1716.

- Progida C, Bakke O (2016). Bidirectional traffic between the Golgi and the endosomes—machineries and regulation. *J Cell Sci* 129, 3971–3982.
- Pulvirenti T, Giannotta M, Capestrano M, Capitani M, Pisanu A, Polishchuk RS, San Pietro E, Beznoussenko GV, Mironov AA, Turacchio G, *et al.* (2008). A traffic-activated Golgi-based signalling circuit coordinates the secretory pathway. *Nat Cell Biol* 10, 912–922.
- Raina K, Noblin DJ, Serebrenik YV, Adams A, Zhao C, Crews CM (2014). Targeted protein destabilization reveals an estrogen-mediated ER stress response. *Nat Chem Biol* 10, 957–962.
- Rambourg A, Clermont Y, Hermo L, Segretain D (1987). Tridimensional architecture of the Golgi apparatus and its components in mucous cells of Brunner's glands of the mouse. *Am J Anat* 179, 95–107.
- Reiling JH, Olive AJ, Sanyal S, Carette JE, Brummelkamp TR, Ploegh HL, Starnbach MN, Sabatini DM (2013). A CREB3-ARF4 signalling pathway mediates the response to Golgi stress and susceptibility to pathogens. *Nat Cell Biol* 15, 1473–1485.
- Satoh A, Wang Y, Malsam J, Beard MB, Warren G (2003). Golgin-84 is a rab1 binding partner involved in Golgi structure. *Traffic* 4, 153–161.
- Schindelin J, Arganda-Carreras I, Frise E, Kaynig V, Longair M, Pietzsch T, Preibisch S, Rueden C, Saalfeld S, Schmid B, *et al.* (2012). Fiji: an open-source platform for biological-image analysis. *Nat Methods* 9, 676–682.
- Shorter J, Warren G (2002). Golgi architecture and inheritance. *Annu Rev Cell Dev Biol* 18, 379–420.
- Stanley P (2011). Golgi glycosylation. *Cold Spring Harb Perspect Biol* 3, 1–14.
- Stieber A, Mourelatos Z, Gonatas NK (1996). In Alzheimer's disease the Golgi apparatus of a population of neurons without neurofibrillary tangles is fragmented and atrophic. *Am J Pathol* 148, 415–426.
- Sütterlin C, Hsu P, Mallabiabarrena A, Malhotra V (2002). Fragmentation and dispersal of the pericentriolar Golgi complex is required for entry into mitosis in mammalian cells. *Cell* 109, 359–369.
- Tae HS, Sundberg TB, Neklesa TK, Noblin DJ, Gustafson JL, Roth AG, Raina K, Crews CM (2012). Identification of hydrophobic tags for the degradation of stabilized proteins. *Chembiochem* 13, 538–541.
- Taniguchi M, Nadanaka S, Tanakura S, Sawaguchi S, Midori S, Kawai Y, Yamaguchi S, Shimada Y, Nakamura Y, Matsumura Y, *et al.* (2015). TFE3 is a bHLH-ZIP-type transcription factor that regulates the mammalian Golgi stress response. *Cell Struct Funct* 40, 13–30.
- Tewari R, Bachert C, Linstedt AD (2015). Induced-oligomerization targets Golgi proteins for degradation in lysosomes. *Mol Biol Cell* 26, 4427–4437.
- Trapnell C, Pachter L, Salzberg SL (2009). TopHat: discovering splice junctions with RNA-Seq. *Bioinformatics* 25, 1105–1111.
- Trapnell C, Williams BA, Pertea G, Mortazavi A, Kwan G, van Baren MJ, Salzberg SL, Wold BJ, Pachter L (2010). Transcript assembly and quantification by RNA-Seq reveals unannotated transcripts and isoform switching during cell differentiation. *Nat Biotechnol* 28, 511–515.
- Varki A (1998). Factors controlling the glycosylation potential of the Golgi apparatus. *Trends Cell Biol* 8, 34–40.
- Wang Y, Satoh A, Warren G (2005). Mapping the functional domains of the Golgi stacking factor GRASP65. *J Biol Chem* 280, 4921–4928.
- Yoshida H, Matsui T, Yamamoto A, Okada T, Mori K (2001). XBP1 mRNA is induced by ATF6 and spliced by IRE1 in response to ER stress to produce a highly active transcription factor. *Cell* 107, 881–891.